Magnetic flux periodicity in second order topological superconductors

Suman Jyoti De,[1] Udit Khanna,[2] and Sumathi Rao[1]
[1]*Harish-Chandra Research Institute, HBNI, Chhatnag Road, Jhunsi, Allahabad 211 019, India*
[2]*Raymond and Beverly Sackler School of Physics and Astronomy, Tel-Aviv University, Tel Aviv, 6997801, Israel*

(Received 29 December 2019; revised manuscript received 8 March 2020; accepted 10 March 2020; published 30 March 2020)

The magnetic flux periodicity of $\frac{hc}{2e}$ is a well-known manifestation of Cooper pairing in typical s-wave superconductors. In this paper we theoretically show that the flux periodicity of a two-dimensional second order topological superconductor, which features zero-energy Majorana modes localized at the corners of the sample, is $\frac{hc}{e}$ instead. We further show that the periodicity changes back to $\frac{hc}{2e}$ at the transition to a topologically trivial superconductor, where the Majorana modes hybridize with the bulk states, demonstrating that the doubling of periodicity is a manifestation of the nontrivial topology of the state.

DOI: 10.1103/PhysRevB.101.125429

I. INTRODUCTION

Topological insulators and superconductors are examples of symmetry-protected topological phases (SPTs) which feature a gapped bulk spectrum with gapless modes localized at the boundaries [1–3]. Free-fermion SPTs with internal symmetries, such as charge conjugation or time reversal, can be completely classified in any dimension on the basis of which ones are present in the system [4–6]. Recent years have seen the advent of new classes of SPTs with spatial or crystalline symmetries. These systems have a much richer connection between the topological properties of the bulk and the states at the boundary. While crystalline topological insulators [7,8] are analogous to the standard SPTs with a gapped bulk and gapless boundaries, higher-order topological phases [9–29] have a gapped bulk with boundaries which are themselves topologically nontrivial. The nth order topological phase in d dimensions has gapless modes at its $(d-n)$-dimensional boundary.

Higher order topological insulators are best understood in the framework of the dipole moment theory of SPTs [11,12]. In this theory, the dipole moment of a crystal is defined in terms of Berry's phase, and the quantization (in the presence of certain symmetries) of this moment leads to topological insulators with boundary charges. This idea can be generalized to higher multipole moments, such as the quadrupole and octopole moments defined in terms of nested Wilson loops [30]. Again, in the presence of certain crystalline symmetries, these moments are quantized and lead to higher order topological insulators with boundary charges at the hinges or the corners. A topological invariant characterizing the higher order TIs can be obtained from the Wilson loops in the same way as one obtains the topological invariant from the Floquet operator, familiar in the context of periodically driven systems [11,12,31].

Second order topological superconductors, in analogy with higher order topological insulators, can be written in terms of a mean-field Bogoliubov–de Gennes (BdG) Hamiltonian describing the bulk gapped d-dimensional superconductor with gapless $d-2$ edge states, instead of $(d-1)$-dimensional edge states as for the usual topological superconductors.

The standard one-dimensional topological superconductors [2,32–34] host edge Majorana modes, which are expected to obey non-Abelian statistics and hence to be relevant for quantum computation. They have been shown [35,36] to exhibit the fractional Josephson effect, where the current-phase relation has a 4π, rather than a 2π, periodicity. Other attempts to probe the topological order includes using a nonlinear Coulomb blockade using a superconducting nanoring [37,38], tunneling spectroscopy [39,40], and transport experiments [41]. There have also been proposals to measure the flux periodicity in a ring geometry with either a single [42] or multiple [43–45] Majorana modes. An alternate system is the chiral p-wave superconductor, which is predicted to occur when the chiral edge modes of a quantum anomalous Hall insulator turn superconducting via the proximity effect [46] and lead to chiral Majorana states, and there has been some experimental evidence [47,48] of these modes. However, it has proved remarkably difficult to unambiguously prove the existence of these Majorana modes.

In this paper, we focus on a two-dimensional second order topological superconductor which hosts zero-energy Majorana modes localized at the corners of the sample. We study the flux periodicity of the superconducting state after introducing a vortex in the center of the sample. The vortex makes the geometry multiply connected, and thus, the superconducting phase winds around the vortex in a nontrivial way. To take this into account, we compute the ground state of the mean-field BdG Hamiltonian self-consistently at each value of the flux. This self-consistent calculation shows us that the flux periodicity of the second order topological superconductor is $\frac{hc}{e}$ instead of $\frac{hc}{2e}$ as expected for a superconductor. To probe the origin of this period doubling, we compute the flux periodicity while varying a parameter in the Hamiltonian which drives the system into a topologically trivial phase. Interestingly, we find that the flux periodicity changes to $\frac{hc}{2e}$ across this transition, proving that the change in flux periodicity is related to the topologically nontrivial nature of the state.

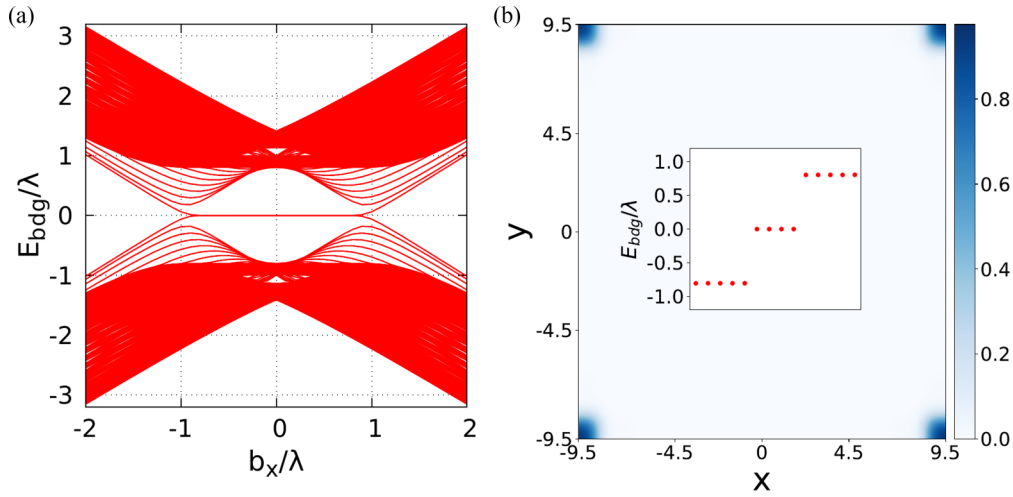

FIG. 1. (a) Plot of the spectrum of the Hamiltonian in Eq. (1) for a 20×20 lattice for open boundary conditions in both directions with respect to the field b_x, which clearly shows the zero modes for $|b_x| < \lambda$. Parameter values are $\lambda = 1$, $\Delta/\lambda = 0.8$ and lattice spacing $a = 1$. (b) Plot of the electron densities which shows the four localized Majorana modes at the four corners. The inset shows four zero-energy modes clearly distinguishable from the bulk spectrum at $b_x = 0$.

The plan of the paper is as follows. In Sec. II, we introduce the model, originally studied in Ref. [49], with p_x+ip_y pairing in a doped Dirac semimetal with two mirror symmetries, i.e., four mirror-symmetric Dirac nodes. We will then show, using a concrete pairing mechanism, that a second order topological superconductor (TSC_2) can be self-consistently realized in such a model, with four Majorana corner modes. We will then introduce a vortex through the center in an annulus geometry (a square annulus in the lattice model) and obtain the self-consistent solutions of the superconducting order parameter as a function of the parameters of the theory. In Sec. III, we will study the energy levels and the circulating current due to the insertion of the vortex and show that the flux periodicity changes from hc/e to $hc/2e$ as a tunable parameter in the model is changed. Further tuning of the parameter to bring the system into the metallic regime changes the flux periodicity back to hc/e, as expected for an Aharonov-Bohm ring. Finally, in Sec. IV, we end with a discussion and conclusions.

II. MODEL AND VORTEX INTRODUCTION

A. Second order topological superconductor

We start with the four-band Bogoliubov–de Gennes model introduced in Ref. [49] with $H = \int d\mathbf{k}\Psi_{\mathbf{k}}^{\dagger}\mathcal{H}(\mathbf{k})\Psi_{\mathbf{k}}$,

$$\mathcal{H}(\mathbf{k}) = [b_x + \lambda\cos(k_x)]\tau_z\sigma_x + \lambda\cos(k_y)1_\tau\sigma_y + \Delta\sin(k_x)\tau_y\sigma_x + \Delta\sin(k_y)\tau_x\sigma_x, \quad (1)$$

and $\Psi_{\mathbf{k}}^{\dagger} = (c_{\mathbf{k}\uparrow}^{\dagger}, c_{\mathbf{k}\downarrow}^{\dagger}, c_{-\mathbf{k}\uparrow}, c_{-\mathbf{k}\downarrow})$. Here, σ (τ) denotes the operators acting on spin (Nambu) space, and 1_τ represents the identity in the Nambu space. λ denotes the hopping. This model can be shown [49] to describe a higher order topological $p_x + ip_y$ superconductor phase for a fixed Δ when $|b_x/\lambda| < 1$, with four Majorana modes localized at the four corners of the sample. This Hamiltonian has a particle-hole symmetry, with τ_x being the charge conjugation operator such that $\tau_x\mathcal{H}(\mathbf{k})^T\tau_x^{-1} = -\mathcal{H}(-\mathbf{k})$. Provided that we choose the pairing terms to have p_x+ip_y symmetry, the model also has two mirror symmetries, $M_x = \sigma_y\tau_y$ and $M_x = \sigma_y\tau_x$, such that $M_{x,y}\mathcal{H}(\mathbf{k})M_{x,y}^{-1} = H(\hat{m}_{x,y}\mathbf{k})$, with the two mirror symmetries anticommuting with each other. More specifically, $M_xH(k_x, k_y)M_x^{-1} = H(-k_x, k_y)$, with similar notation for M_y.

This model has a gapped spectrum, but as shown in Ref. [49], for $|b_x| < \lambda$, the model denotes a TSC_2; that is, the edge states themselves are topological and have gapless corner states. Analogous to what was done for the model of higher order topological insulators in Ref. [12], we can plot the spectrum for open boundary conditions in both the x and y directions, parametrically, as a function of b_x, as shown in Fig. 1. The spectrum in Fig. 1(a) clearly shows the existence of zero modes for $|b_x/\lambda| < 1$, and in Fig. 1(b), the densities clearly show four localized modes at the four corners of the lattice.

A two-dimensional quadrupole insulator can be characterized by a quantized quadrupole moment Q as argued in Refs. [11,50,51], and the quadrupole moment is defined as a ground state $|\Phi_0\rangle$ expectation value of a many-body operator as follows:

$$Q = \frac{e}{2\pi}\mathrm{Im}[\ln(\langle\Phi_0|\hat{O}|\Phi_0\rangle)] \text{ (modulo 1)},$$
$$\hat{O} = \exp\left(2\pi i\frac{1}{L_xL_y}\sum_{x,y}xy\,\hat{n}(x,y)\right), \quad (2)$$

where (x, y) is the lattice site index, $\hat{n}(x, y)$ is the quasiparticle density at the site (x, y), and L_x, L_y are the lengths of the $2d$ system. By analogy, we can define a similar quadrupole moment for the two-dimensional topological superconductor, which has been plotted in Fig. 2. The quadrupole moment shows a sharp transition from $Q = 0.5$ to $Q = 0$ at the value of b_x where the model transitions from a topological superconductor into a normal superconductor. This transition occurs close to $b_x/\lambda = 1$. This is also consistent with the disappearance of the corner Majorana modes at $b_x = 1$ as seen in Fig. 1. Here and in Fig. 2(a), the minor deviation from unity is a finite-size effect. Note, however, that the density plotted

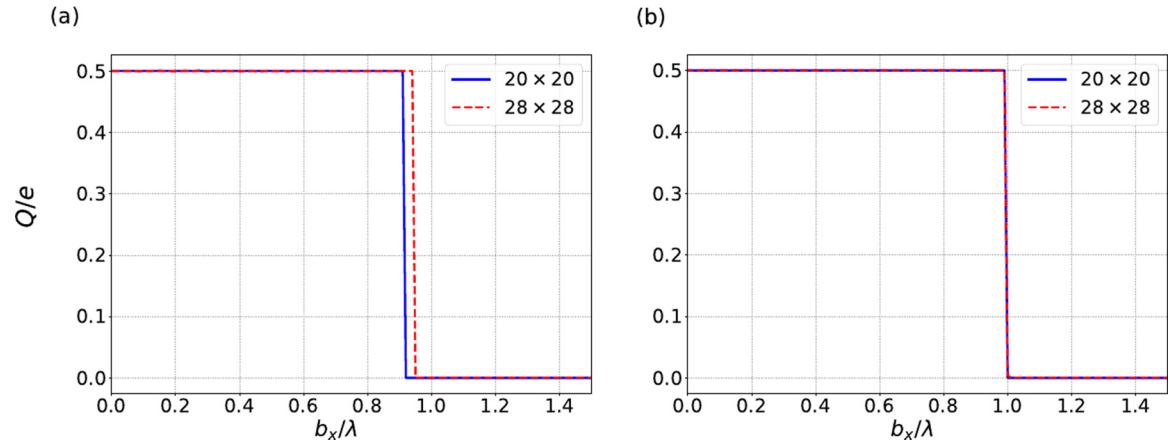

FIG. 2. The quadrupole moment Q as a function of b_x/λ for the Hamiltonian in Eq. (1) with $\lambda = 1$, $\Delta/\lambda = 0.8$, and lattice spacing $a = 1$. (a) For open boundary conditions in both the x and y directions and (b) for open boundary conditions in the y direction and periodic boundary conditions in the x direction. This shows that the second order topological superconductor phase has $Q/e = 0.5$ (modulo 1) and the topologically trivial phase has $Q/e = 0.0$ (modulo 1). The phase transition from a topological to a nontopological superconducting phase occurs at $b_x/\lambda = 1.0$ in (b), showing that the minor deviation from unity in (a) here as well as in Fig. 1(a) is a finite-size effect.

in the figure is that of the bogoliubons, linear combinations of the particle and hole operators obtained by diagonalizing the Hamiltonian in Eq. (1) with the pairing term Δ. This is discussed further in the next section, where we compute the quadruple moment with a self-consistent pairing term.

The normal state of this Hamiltonian (when $\Delta = 0$) has four gapless mirror-symmetric Dirac points, and it can be shown that at a finite chemical potential, regions of the Fermi surface with opposite momenta always have the same spin texture. Hence, it is natural [49] for a spin triplet superconducting gap to be induced by electronic interactions. The pairing potential Δ_{ij} with the appropriate p_x+ip_y symmetry can be derived from a mean-field treatment of the pairing interaction

$$H_{int} = \frac{V}{2}\sum_{\langle i,j\rangle}(n_{i\uparrow}n_{j\downarrow} + n_{i\downarrow}n_{j\uparrow}), \tag{3}$$

where $\langle i, j\rangle$ denotes nearest-neighbor sites. We will show in a later section that Δ_{ij} can be obtained self-consistently for our model on a square lattice.

B. Vortex insertion in an annulus geometry

The basic idea is that in a superconducting ring, the order parameter responds to a flux or vortex inserted through the ring. Just as a current through a metallic ring is modulated by an hc/e periodicity due to the Aharonov-Bohm effect, the current through a superconducting ring is expected to be modulated as $hc/2e$ [52,53]. Although naively explained in terms of the Cooper pair condensates having a charge of $2e$, the theoretical explanation is more subtle and comes from the degeneracy between two different classes of superconducting wave functions at $\phi = 0$ and at $\phi = \phi_0/2$. The first class consists of those wave functions with pairing between the angular momentum states $\hbar k$ and $-\hbar k$ leading to Cooper pairs with $\hbar q = 0$. All even values of q can be obtained from these wave functions by gauge transformations. The second class consists of those wave functions with pairing between $\hbar k$ and $\hbar(-k+1)$ leading to Cooper pairs with $\hbar q = 1$, with, again, all odd-integer values of q being related to these wave functions by gauge transformations. Both these classes of wave functions turn out to have the same energy for flux $\phi = 0$ and $\phi = hc/2e$. But more recently, the question of the flux periodicity has resurfaced in the context of high-T_c d-wave superconductors [54], where it was seen that the condensate reconstructs for half-integer flux quanta and breaks the degeneracy between the state at zero flux and the state at half-integer flux. Thus, the periodicity changes back to hc/e as for normal metals. Even for s-wave superconductors, it has been shown [55] that for superconducting rings with a diameter smaller than the coherence length, the response due to magnetic flux is generally modulated as hc/e periodic instead of $hc/2e$.

Here, we study the response in a p_x+ip_y higher order topological superconductor "ring." We imagine adding an infinitely long solenoid (of infinitesimal radius) at the origin of a $2d$ sample so that there is no magnetic field crossing any of the sites, but a closed loop around the origin encloses a flux, thereby mimicking an annulus with flux through the hole. More specifically, we have a square geometry and assume that the lattice sites are located at $\mathbf{r} = (m + 1/2, n + 1/2)$, where m, n are integers from $-L$ to $L - 1$. This ensures that the lattice sites are symmetrically located about the origin at $\mathbf{r} = (0, 0)$. This is shown in Fig. 3.

In the absence of superconductivity, a vortex can be added to $\mathcal{H}$ through the standard Peierls substitution [56]. Under this transformation, the kinetic terms change as follows:

$$\begin{aligned}\psi^\dagger_{\mathbf{r}+\hat{\delta}}\psi_{\mathbf{r}} &\to \psi^\dagger_{\mathbf{r}+\hat{\delta}}\psi_{\mathbf{r}}\exp\left(i\frac{e}{c\hbar}\int_{\mathbf{r}}^{\mathbf{r}+\hat{\delta}} d\mathbf{r}'\cdot\vec{A}(\mathbf{r}')\right)\\ &= \psi^\dagger_{\mathbf{r}+\hat{\delta}}\psi_{\mathbf{r}}\exp\left(i\frac{\phi}{\phi_0}\int_{\mathbf{r}}^{\mathbf{r}+\hat{\delta}} d\mathbf{r}'\cdot\hat{\theta}\frac{1}{|\mathbf{r}'|}\right),\end{aligned} \tag{4}$$

where $\phi_0 = hc/e$, $\psi^\dagger_{\mathbf{r}} = (c^\dagger_{\mathbf{r}\uparrow}, c^\dagger_{\mathbf{r}\downarrow}, c_{\mathbf{r}\uparrow}, c_{\mathbf{r}\downarrow})$, and $\hat{\delta}$ is constrained only up to the nearest neighbor in both the $\hat{x}$ and $\hat{y}$ directions. Every bond of the lattice will clearly pick up a

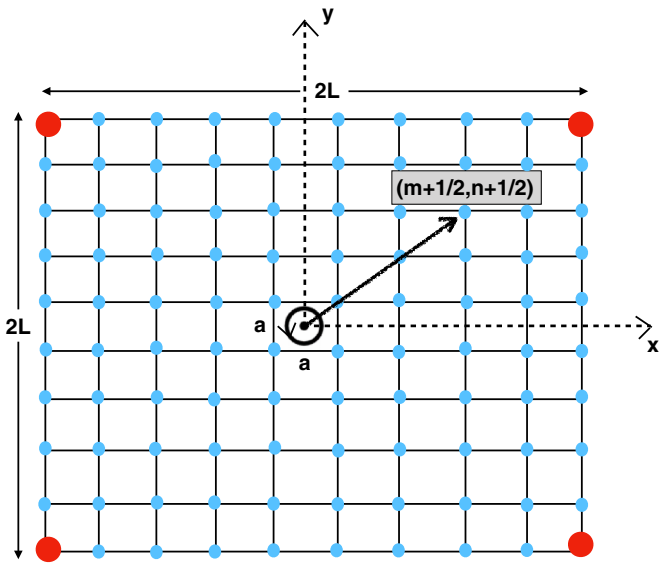

FIG. 3. Schematic diagram of flux insertion through the central plaquette ($a \times a$) of a square lattice ($2L \times 2L$) leading to a ring geometry.

different phase due to the $\frac{\hat{\theta}}{|\mathbf{r}'|}$ in the integral, but at $\phi = n\phi_0$ (where n is an integer), the total phase accumulated by an electron going through each plaquette around the origin is $2\pi n$. Therefore, the system behaves as if there is no magnetic field at all. For illustration, the lowest three positive and negative eigenvalues are shown as a function of the flux in Fig. 4, which shows that the spectrum is $\phi_0 = \frac{hc}{e}$ periodic, as expected.

However, in the presence of pairing terms ($\Delta \neq 0$), adding a flux or creating a vortex at the center of the system makes Δ position dependent, and keeping it constant is no longer viable. We need to solve for Δ self-consistently, which is done in the next section.

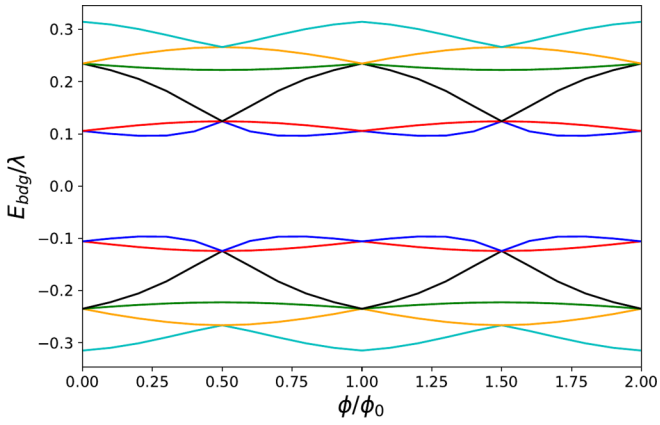

FIG. 4. Lowest three positive and negative eigenvalues of the Hamiltonian in Eq. (1) for a 20×20 lattice, showing their magnetic flux periodicity, as a function of the flux ϕ/ϕ_0 introduced at the origin. $\phi_0 = hc/e$. The parameter values are $\lambda = 1$, $\Delta = 0$, $b_x/\lambda = 0$, and lattice spacing $a = 1$.

III. SELF-CONSISTENT CALCULATION AND RESULTS

We work with the Hamiltonian in Eq. (1) in real space, given by

$$\mathcal{H} = \sum_{\langle i,j \rangle} \left(\mathcal{H}^0_{ij} c^\dagger_{i\uparrow} c_{j\downarrow} + \text{H.c.}\right) + \sum_{\langle i,j \rangle} (\Delta_{ij} c^\dagger_{i\uparrow} c^\dagger_{j\downarrow} + \Delta^*_{ji} c_{i\downarrow} c_{j\uparrow}), \tag{5}$$

where $\mathcal{H}^0_{ij} = \vec{t_h} \exp(i\phi_{ij}) + 2b_x\delta_{ij}$, with $t^x_h = \lambda$ and $t^y_h = -i\lambda$, are the hopping matrix elements between the nearest-neighbor sites. Also $\phi_{ij} = \int_{\mathbf{r}_j}^{\mathbf{r}_i} \frac{e}{\hbar c}[\vec{A}(\mathbf{r}') \cdot d\vec{\mathbf{r}}']$ is the Peierls phase factor coming from $\vec{A}(\mathbf{r})$, which is the vector potential due to flux through the origin. The order parameter of the superconducting state Δ_{ij} is defined on the links between neighboring sites with the appropriate p-wave symmetry; that is, we have

$$\Delta_{ij} = \frac{V}{2}[\langle c_{i\uparrow} c_{j\downarrow} \rangle + \langle c_{i\downarrow} c_{j\uparrow} \rangle], \tag{6}$$

which is symmetric under the exchange of spins and antisymmetric under the exchange of spatial indices. Here, V is the nearest-neighbor pairing interaction strength. Now following a Bogoliubov rotation and in terms of the new fermionic operators (the bogoliubons) γ_n,

$$c_{i\sigma} = \sum_n \left[u^n_{i\sigma} \gamma_n - \left(v^n_{i\sigma}\right)^* \gamma^\dagger_n\right], \tag{7}$$

we find that the Hamiltonian in Eq. (5) is given by

$$\mathcal{H} = E_g + \sum_n (E_n \gamma^\dagger_n \gamma_n), \quad E_n > 0, \tag{8}$$

with $E_g = -\sum_{i,\sigma,n} E_n |v^n_{i\sigma}|^2$, where the coefficients (u^n) and (v^n) satisfy the equation

$$\begin{pmatrix} \mathcal{H}^0 & -\Delta \\ -\Delta^\dagger & -\mathcal{H}^{0T} \end{pmatrix} \begin{pmatrix} u^n \\ v^n \end{pmatrix} = E_n \begin{pmatrix} u^n \\ v^n \end{pmatrix}. \tag{9}$$

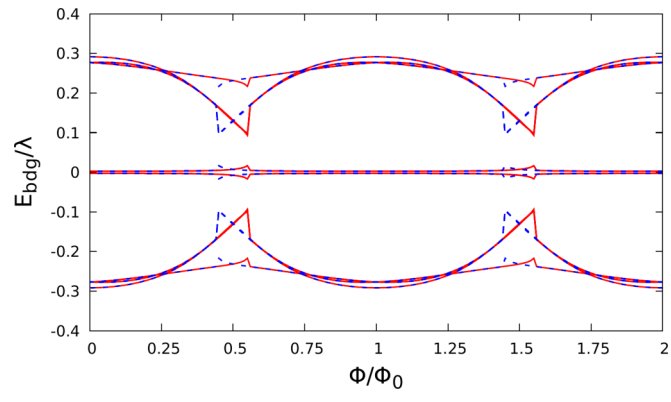

FIG. 5. Self-consistent lowest three positive and negative eigenvalues of the Hamiltonian in Eq. (5) for a 20×20 lattice as a function of the flux ϕ/ϕ_0 introduced at the origin for $\lambda = 1$, $V = 3\lambda$, $b_x/\lambda = 0$, and lattice spacing $a = 1$. Note the existence of two different self-consistent states (one is the solid red line, and the other one is the dashed blue line) close to $\phi = \phi_0/2$.

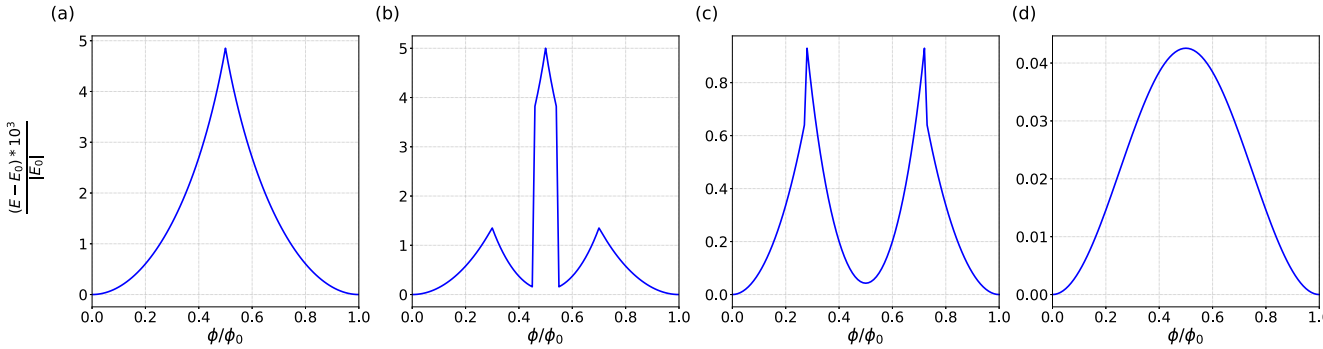

FIG. 6. Self-consistent total energy $\{[E(\phi/\phi_0) - E(0)] \times 10^3\}/|E(0)|$ as a function of the flux ϕ/ϕ_0 through the center of a 20×20 square lattice with lattice spacing $a = 1$ for the Hamiltonian in Eq. (5). The parameters chosen are $\lambda = 1$ and $V = 3\lambda$, with (a) $b_x/\lambda = 0.0$, (b) $b_x/\lambda = 0.3$, (c) $b_x/\lambda = 0.8$, and (d) $b_x/\lambda = 1.5$. Note that the flux periodicity changes from ϕ_0 to $\phi_0/2$ and back again to ϕ_0 as b_x is tuned.

Here, (u^n) and (v^n) are $2N$-dimensional column vectors (N is the total number of lattice sites, and the $2N$ is because of spin), and both $\mathcal{H}^0$ and Δ are $2N \times 2N$ matrices. The order parameter $\Delta_{ij}(\phi, b_x)$ is then calculated self-consistently from

$$\Delta_{ij} = \frac{V}{4}\sum_n \Big[u^n_{j\uparrow}(v^n_{i\downarrow})^* + u^n_{j\downarrow}(v^n_{i\uparrow})^* - u^n_{i\uparrow}(v^n_{j\downarrow})^* - u^n_{i\downarrow}(v^n_{j\uparrow})^*\Big] \tanh\left(\frac{E_n}{2k_BT}\right), \quad E_n > 0, \tag{10}$$

and is used to compute the energy eigenvalues and the total energy.

In Fig. 5, we show the self-consistent energy eigenvalues in the presence of a vortex for a finite pairing interaction. We can compare these energy eigenvalues with those in Fig. 4 without the pairing term and note that there are four zero-energy modes well separated from the bulk states, clearly showing that the system is a second order topological superconductor. Moreover, the spectrum surprisingly shows a magnetic flux periodicity of $\frac{hc}{e}$ as opposed to a magnetic flux periodicity of $\frac{hc}{2e}$ in a typical s-wave superconductor.

The total self-consistent energy is shown in Fig. 6 for four different values of b_x/λ as a function of the flux ϕ/ϕ_0 through the center of the lattice. The total energy initially has a maximum at $\phi = \phi_0/2$ at $b_x = 0$ which is in the topological superconductor regime, as shown in Fig. 6(a). But as b_x increases, we note that the width of the maximum reduces [as in Fig. 6(b)], and then as shown in Fig. 6(c), the total energy develops a minimum at $\phi = \phi_0/2$. Finally, in Fig. 6(d), we note that at even higher values of b_x where the model is no longer in the topological superconductor regime, the minimum at $\phi = \phi_0/2$ is again replaced by a maximum. So as one increase b_x from $b_x/\lambda = 0$, the magnetic flux periodicity of the total energy which was ϕ_0 to start with goes to $\phi_0/2$ at intermediate b_x and then goes back again to ϕ_0 as one further increases b_x.

Note that we have fixed the chemical potential at $\mu = 0$ and have occupied two of the zero-energy states; that is, we are in the even-parity state. As we change the flux, we keep the total number of particles fixed (the band has been precisely half filled). So we are in the Coulomb blockaded regime where the parity of the state cannot change and continues to remain even.

The lattice current density $\vec{J}_{ij}$ from lattice site i to j is then obtained as

$$\vec{J}_{ij} = -\frac{2e}{\hbar}\mathrm{Im}[\vec{t}_h\langle c^\dagger_{j\uparrow}c_{i\downarrow}\rangle \exp(i\phi_{ji}) - \vec{t}_h\langle c^\dagger_{i\uparrow}c_{j\downarrow}\rangle \exp(i\phi_{ij})] \tag{11}$$

using the continuity equation which is then used to compute the total circulating current in the system, which is shown in

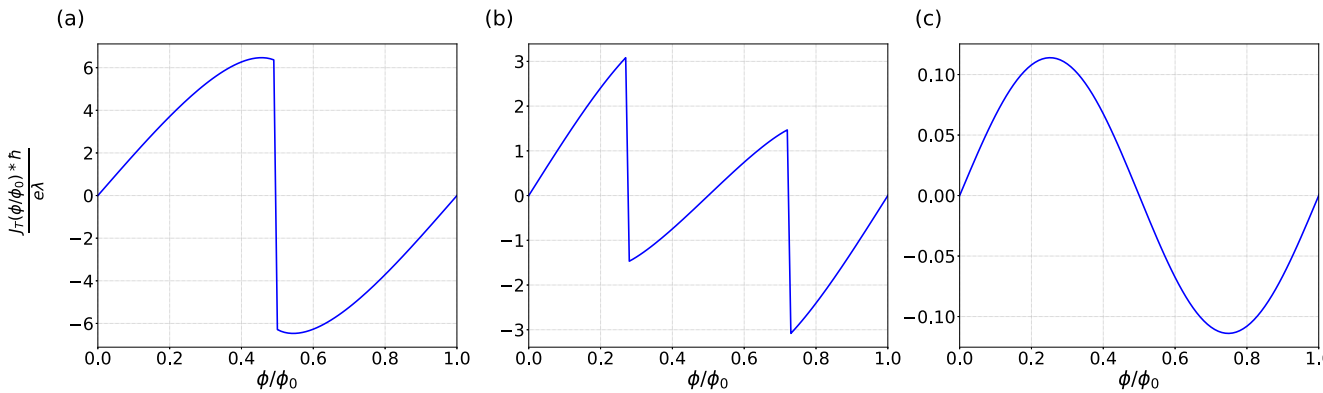

FIG. 7. Total circulating current $J_T(\phi/\phi_0)$ as a function of flux ϕ/ϕ_0 through the center of a 20×20 square lattice with lattice spacing $a = 1$ for the Hamiltonian in Eq. (5). $\lambda = 1$ and $V = 3\lambda$ as in Fig. 6. Note that the flux periodicity is ϕ_0 in (a) with $b_x/\lambda = 0.0$, $\phi_0/2$ in (b) with $b_x/\lambda = 0.7$, and is again back to ϕ_0 in (c) with $b_x/\lambda = 1.5$.

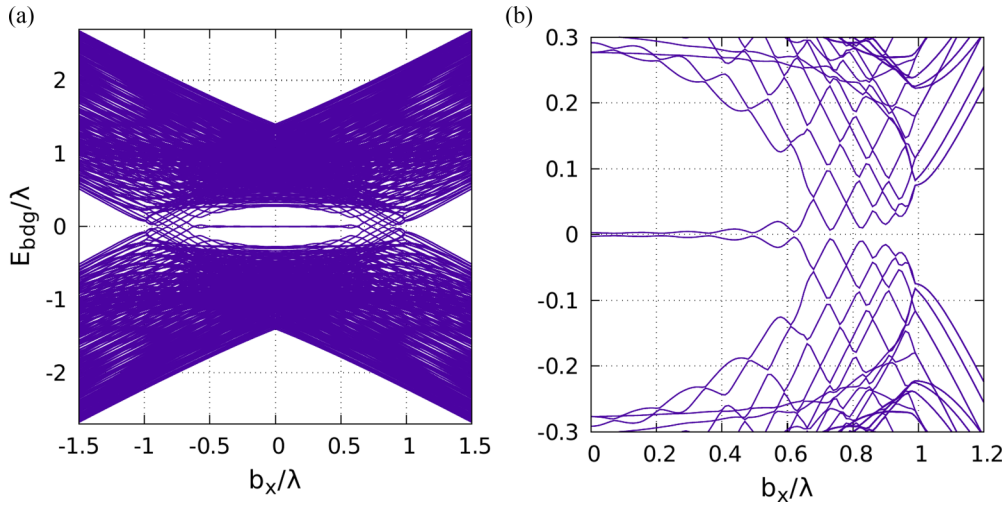

FIG. 8. Self-consistent spectrum for the Hamiltonian in Eq. (5) on a 20×20 square lattice with lattice spacing $a = 1$, without any flux as a function of field b_x/λ for $\lambda = 1, V = 3\lambda$. (a) The full spectrum and (b) the spectrum close to zero energy. These plots show that close to $b_x/\lambda \simeq 0.6$ zero energy is gapped out by mixing with the bulk energy, giving an indication that there is a phase transition at that point.

Fig. 7. Here again, we note that as b_x increases, there is a tendency towards period doubling; that is, the flux periodicity changes from ϕ_0 to $\phi_0/2$. A further increase in b_x brings the periodicity again back to ϕ_0, as shown in Fig. 7(c). Note however, that both the energy and the current density show only the tendency towards $\phi_0/2$ periodicity. Neither of them are exactly $\phi_0/2$ periodic. This is because we have a finite system with a small gap in the normal superconducting region, and it is known that in the small-gap regime, one does not get perfect $\phi_0/2$ periodicity [55].

Now to see why the magnetic flux periodicity of the system changes from ϕ_0 to $\phi_0/2$ and goes back again to ϕ_0, we have calculated the self-consistent spectrum in the absence of the vortex but as a function of b_x/λ, as illustrated in Fig. 8. The spectrum clearly shows that for small enough b_x/λ, there are zero-energy states well separated from the bulk states. Here, the system is in a second order topological superconductor phase and the magnetic flux periodicity of this topological phase is $\frac{hc}{e}$, as seen in the total energy in Fig. 6(a) and in the total circulating current in Fig. 7(a). Now close to $b_x/\lambda \simeq \pm 0.6$, the bulk energy gap closes, and the zero-energy states mix with bulk states, giving rise to a continuum of energy states and signifying a change in the topology of the system.

We have also calculated the site average of the pairing term as a function of b_x/λ as illustrated in Fig. 9 to show that the system has finite pairing term up to $b_x/\lambda \simeq 1.0$. So the system remains in a superconducting phase up to $b_x/\lambda \simeq 1.0$; however, close to $b_x/\lambda \simeq 0.6$ there is a phase transition from a topological to a nontopological superconductor, which can be seen from the vanishing of the zero-energy states. This causes the magnetic flux periodicity to change from $\frac{hc}{e}$ to $\frac{hc}{2e}$, which is seen both in the total energy and in the total circulating current in the system. So the magnetic flux periodicity change from $\frac{hc}{e}$ to $\frac{hc}{2e}$ is associated with the change in topology of the system; that is, the second order topological superconductor has a flux periodicity of $\frac{hc}{e}$ in contrast to a nontopological superconductor, which has a flux periodicity of $\frac{hc}{2e}$. When b_x is increased beyond $b_x/\lambda \simeq 1.0$, the pairing term goes to zero, and the system is in the metallic phase. This again explains the switch back to the magnetic flux periodicity of $\frac{hc}{e}$, as seen both in the total energy in Fig. 6(d) and in the total persistent current in Fig. 7(c). This is just the expected periodicity due to the Aharonov-Bohm effect when a flux is inserted through a metallic ring.

We also confirm the phase transition from a topological superconductor to a normal superconductor at $b_x/\lambda \sim 0.6$ by calculating the the quadrupole moment (Q/e) using the definition given in Eq. (2) for the Hamiltonian in Eq. (5) without any flux. As outlined in Ref. [25], we construct the state $|\Phi_0\rangle$ for the half-filled system and then take the average of the operator $\hat{O}$ defined in Eq. (2). However, here the filling refers to the filling of bogoliubons as defined in Eqs. (7) and (8). As shown in Fig. 10(b) for low values of b_x, the system is in the second order topological superconductor phase, and the quadrupole moment is nonzero and given by $Q/e = 0.5$ (modulo 1). But at $b_x/\lambda \simeq 0.6$, Q/e becomes 0 (modulo 1),

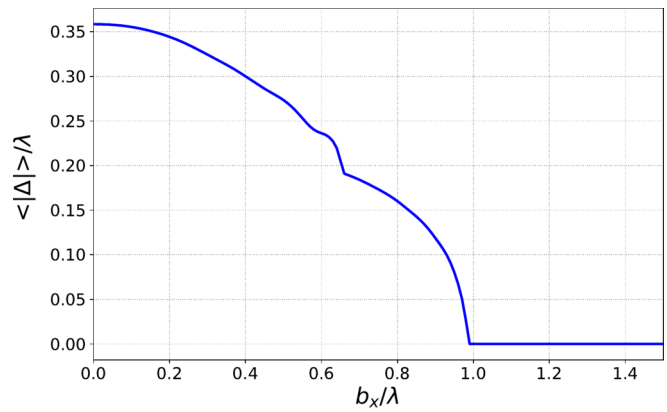

FIG. 9. Site average of the pairing term $\langle|\Delta|\rangle$ as a function of b_x/λ, calculated self-consistently without flux for the Hamiltonian in Eq. (5) on a 20×20 square lattice for $\lambda = 1, V = 3\lambda$ and lattice spacing $a = 1$. This clearly shows that the system is in a superconducting phase until $b_x \sim 1.0$. A further increase of b_x brings the system to a nonsuperconducting phase with zero pairing.

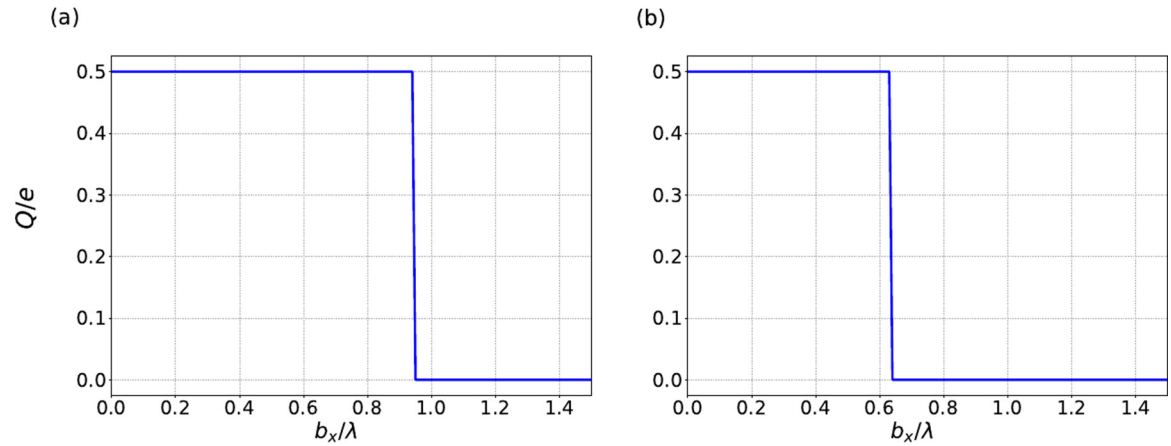

FIG. 10. The quadrupole moment Q/e as a function of the field b_x/λ for (a) $\Delta/\lambda = 0.4$ (without self-consistency) for the Hamiltonian in Eq. (1) and for (b) $V = 3\lambda$ (using self-consistency) for the Hamiltonian in Eq. (5) for $\lambda = 1$, flux $\phi = 0$, and a 20×20 square lattice with lattice spacing $a = 1$ with open boundary conditions in both the x and y directions. In (b), the transition to a nontopological phase occurs at $b_x/\lambda \simeq 0.6$, in contrast to (a), where the transition happens at $b_x/\lambda \simeq 1.0$.

indicating that the system transitions to the nontopological superconductor phase. This is consistent with the spectrum, which also shows a gap closing at the same point. This confirms that the change in the magnetic flux periodicity from $\frac{hc}{e}$ to $\frac{hc}{2e}$ close to $b_x/\lambda \simeq 0.7$ for the system shown in Figs. 6(c) and 7(b) is associated with the change in the topology of the system.

Note that the change in periodicity can also be understood in a simple one-particle picture in the following way. As mentioned in Sec. II B, for normal s-wave superconductors, there are two classes of pairing wave functions: the class-I wave functions, where the pairing is between $\hbar(+k)$ and $\hbar(-k)$ at $\phi = 0$, and the class-II pairing wave functions, where the pairing is between $\hbar(+k)$ and $\hbar(-k+1)$ at $\phi = \phi_0/2$. The pairing energy is exactly the same for both these classes of wave functions, so there is perfect degeneracy between the ground-state energy at $\phi = 0$ and at $\phi = \phi_0/2$. This is what leads to the $\phi_0/2$ periodicity of a normal s-wave superconducting ring. However, for a weak-pairing p-wave superconductor, the orbital antisymmetry does not allow two electrons in the $k = 0$ state at $\phi = 0$. Thus, there are unpaired electrons at $k = 0$ and at the Fermi energy, so one pair of electrons remains unpaired, as shown in Fig. 11(a). However, at $\phi = \phi_0/2$, the energy minimum shifts, and the pairings are now the class-II pairings, which allows for equal-energy pairings for all values of momenta. This is illustrated in Fig. 11(c). This breaks the exact degeneracy between the ground states at $\phi = 0$ and $\phi = \phi_0/2$. Thus, for p-wave topological superconductors, which are weak-pairing p-wave superconductors, the periodicity is ϕ_0 and not $\phi_0/2$.

However, for $b_x > 0.6$, where our results show that there is a phase transition from a topological to nontopological superconductor, it is likely that the transition is to the strong-pairing p-wave phase where the pairing can occur even between states that are slightly different in energy, as shown in Fig. 11(b). In that case, even at $\phi = 0$, all states are paired, and the degeneracy between the ground states at $\phi = 0$ and $\phi = \phi_0/2$ is restored.

We also note that a similar result of period doubling in the semiconductor-superconductor nanowires with $p + ip$ superconductivity was previously studied by Zocher *et al.* [37,38]. For even parity, they also showed that for fixed mean particle number, the excitation spectrum showed clear signatures of the $\frac{hc}{e}$ periodicity in the topologically nontrivial phase.

IV. DISCUSSION AND CONCLUSIONS

In this work, we have focused on the magnetic flux periodicity of a second order topological superconductor in two dimensions with four Majorana modes at the corners. By implementing a ring geometry via a flux at the origin, we show that the flux periodicity changes from $\frac{hc}{e}$ to $\frac{hc}{2e}$ when the topological superconductor transitions to an ordinary superconductor.

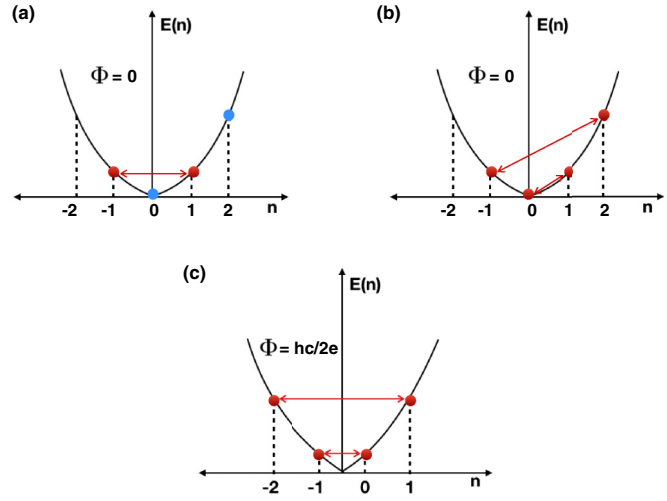

FIG. 11. One-particle energy levels of electrons on a ring. (a) Equal-energy class-I pairing at $\phi = 0$, relevant for weak-pairing p-wave topological superconductors. Note that the states at $\hbar k = 0$ and $\hbar k = 2$ are unpaired. (b) Unequal-energy class-II pairings relevant to strong-coupling superconductors (for $b_x > 0.6$). (c) Equal-energy class-II pairings at $\phi = \phi_0/2$, relevant for both weak- and strong-pairing p-wave cases. (The red dot with the two-headed arrow denotes paired electrons, and the blue dot is for an unpaired electron.)

This model hosts four Majorana modes at its corners, which is sufficient to exploit their non-Abelian nature in braiding since they can be paired in different ways [57]. By insertion of multiple vortices and generalizing our model, one can expect to braid the Majorana modes through adiabatic manipulations of fluxes. This could be useful in designing non-Abelian quantum computational protocols. Therefore, higher order topological insulators could open a new pathway towards topological quantum computation.

ACKNOWLEDGMENTS

U.K. was supported by the Raymond and Beverly Sackler Faculty of Exact Sciences at Tel Aviv University and the Raymond and Beverly Sackler Center for Computational Molecular and Material Science. We thank A. Agarwala, S. Kadge, G. Murthy, B. Rosenow, and Y. Gefen for useful discussions.

[1] M. Z. Hasan and C. L. Kane, Rev. Mod. Phys. **82**, 3045 (2010).
[2] X.-L. Qi and S.-C. Zhang, Rev. Mod. Phys. **83**, 1057 (2011).
[3] B. A. Bernevig, *Topological Insulators and Topological Superconductors* (Princeton University Press, Princeton, NJ, 2013).
[4] A. P. Schnyder, S. Ryu, A. Furusaki, and A. W. W. Ludwig, in *Advances in Theoretical Physics: Landau Memorial Conference*, AIP Conf. Proc. No. 1134 (AIP, New York, 2009), p. 10.
[5] A. Kitaev, in *Advances in Theoretical Physics: Landau Memorial Conference*, AIP Conf. Proc. No. 1134 (AIP, New York, 2009), p. 22.
[6] S. Ryu, A. P. Schnyder, A. Furusaki, and A. W. W. Ludwig, New J. Phys. **12**, 065010 (2010).
[7] P. Dziawa, B. Kowalski, K. Dybko, R. Buczko, A. Szczerbakow, M. Szot, E. Lusakowska, T. Balasubramanian, B. M. Wojek, and M. Berntsen, Nat. Mater. **11**, 1023 (2012).
[8] Y. Tanaka, Z. Ren, T. Sato, K. Nakayama, S. Souma, T. Takahashi, K. Segawa, and Y. Ando, Nat. Phys. **8**, 800 (2012).
[9] W. A. Benalcazar, J. C. Y. Teo, and T. L. Hughes, Phys. Rev. B **89**, 224503 (2014).
[10] R. J. Slager, L. Rademaker, J. Zaanen, and L. Balents, Phys. Rev. B **92**, 085126 (2015).
[11] W. A. Benalcazar, B. A. Bernevig, and T. L. Hughes, Science **66**, 61 (2017).
[12] W. A. Benalcazar, B. A. Bernevig, and T. L. Hughes, Phys. Rev. B **96**, 245115 (2017).
[13] J. Langbehn, Y. Peng, L. Trifunovic, F. von Oppen, and P. W. Brouwer, Phys. Rev. Lett. **119**, 246401 (2017).
[14] J. Kruthoff, J. de Boer, J. van Wezel, C. L. Kane, and R. J. Slager, Phys. Rev. X **7**, 041069 (2017).
[15] F. Schindler, A. M. Cook, M. G. Vergniory, Z. Wang, S. S. P. Parkin, B. A. Bernevig, and T. Neupert, Sci. Adv. **4**, 346 (2018).
[16] Z. Song, Z. Fang, and C. Fang, Phys. Rev. Lett. **119**, 246402 (2017).
[17] C. Fang and L. Fu, arXiv:1709.01929.
[18] E. Khalaf, H. C. Po, A. Vishwanath, and H. Watanabe, Phys. Rev. X **8**, 031070 (2018).
[19] M. Geier, L. Trifunovic, M. Hoskam, and P. W. Brouwer, Phys. Rev. B **97**, 205135 (2018).
[20] E. Khalaf, Phys. Rev. B **97**, 205136 (2018).
[21] R. Queiroz and A. Stern, Phys. Rev. Lett. **123**, 036802 (2019).
[22] L. Trifunovic and P. W. Brouwer, Phys. Rev. X **9**, 011012 (2019).
[23] R. Seshadri, A. Dutta, and D. Sen, Phys. Rev. B **100**, 115403 (2019).
[24] S. A. A. Ghorashi, X. Hu, T. L. Hughes, and E. Rossi, Phys. Rev. B **100**, 020509(R) (2019).
[25] A. Agarwala, V. Juričić, and B. Roy, Phys. Rev. Research **2**, 012067(R) (2020).
[26] T. Nag, V. Juricic, and B. Roy, Phys. Rev. Res. **1**, 032045(R) (2019).
[27] K. Kudo, T. Yoshida, and Y. Hatsugai, Phys. Rev. Lett. **123**, 196402 (2019).
[28] A. Tiwari, M. Li, B. A. Bernevig, T. Neupert, and S. A. Parameswan, Phys. Rev. Lett. **124**, 046801 (2019).
[29] S. A. A. Ghorashi, T. L. Hughes, and E. Rossi, arXiv:1909.10536.
[30] T. Neupert and F. Schindler, in *Topological Matter: Lectures from the Topological Matter School 2017*, edited by D. Bercioux, J. Cayssol, M. G. Vergniory, and M. R. Calvo, *Springer Series in Solid-State Sciences* (Springer International Publishing, Cham, 2018), pp. 31–61.
[31] S. Franca, J. van den Brink, and I. C. Fulga, Phys. Rev. B **98**, 201114(R) (2018).
[32] J. Alicea, Rep. Prog. Phys. **75**, 076501 (2012).
[33] C. Beenakker, Annu. Rev. Condens. Matter. Phys. **4**, 113 (2013).
[34] R. A. Sola, Riv. Nuovo Cimento **40**, 523 (2017).
[35] A. Y. Kitaev, Phys. Usp. **44**, 131 (2001).
[36] H. J. Kwon, K. Sengupta, and V. M. Yakovenko, Eur. Phys. J. B **37**, 349 (2004).
[37] B. Zocher, M. Horsdal, and B. Rosenow, Phys. Rev. Lett. **109**, 227001 (2012).
[38] B. Zocher, M. Horsdal, and B. Rosenow, New J. Phys. **15**, 085003 (2013).
[39] M. Wimmer, A. R. Akhmerov, J. P. Dalhaus, and C. W. Beenakker, New J. Phys. **13**, 053016 (2011).
[40] M. Leijnse and K. Flensberg, Phys. Rev. B **84**, 140501(R) (2011).
[41] S. Tewari, J. D. Sau, V. W. Scarola, C. Zhang and S. Das Sarma, Phys. Rev. B **85**, 155302 (2012).
[42] K. M. Tripathi, S. Das, and S. Rao, Phys. Rev. Lett. **116**, 166401 (2016).
[43] S. Rubbert and A. R. Akhmerov, Phys. Rev. B **94**, 115430 (2016).
[44] C. K. Chiu, J. D. Sau and S. Das Sarma, Phys. Rev. B **97**, 035310 (2018).
[45] C.-X. Liu, W. S. Cole, and J. D. Sau, Phys. Rev. Lett. **122**, 117001 (2019).
[46] X. L. Qi, T. L. Hughes, and S. C. Zhang, Phys. Rev. B **82**, 184516 (2010).
[47] Q. L. He, L. Pan, A. L. Stern, E. C. Burks, X. Che, G. Yin, J. Wang, B. Lian, Q. Zhou, E. S. Choi, K. Murata, X. Kou, Z. Chen, T. Nie, Q. Shao, Y. Fan, S.-C. Zhang, K. Liu, J. Xia, and K. L. Wang, Science **357**, 294 (2017).
[48] J. Shen, J. Lyu, J. Z. Gao, Y.-M. Xie, C.-Z. Chen, C.-W. Cho, O. Atanov, Z. Chen, K. Liu, Y. J. Hu, K. Y. Yip, S. K. Goh, Q.

L. He, L. Pan, K. L. Wang, K. T. Law, and R. Lortz, Proc. Natl. Acad. Sci. **117**, 238 (2020).
[49] Y. Wang, M. Lin, and T. L. Hughes, Phys. Rev. B **98**, 165144 (2018).
[50] W. A. Wheeler, L. K. Wagner, and T. L. Hughes, Phys. Rev. B **100**, 245135 (2019).
[51] B. Kang, K. Shiozaki, G. Y. Cho, Phys. Rev. B **100**, 245134 (2019).
[52] N. Byers and C. N. Yang, Phys. Rev. Lett. **7**, 46 (1961).
[53] L. Onsager, Phys. Rev. Lett. **7**, 50 (1961).
[54] F. Loder, A. P. Kampf, T. Kopp, J. Mannhart, C. W. Schneider, and Y. S. Barash, Nat. Phys. **4**, 112 (2008).
[55] F. Loder, A. P. Kampf, and T. Kopp, in *Superconductivity: Materials, Properties and Applications*, edited by A. Gabovich (InTech, Rijeka, Croatia, 2012), Chap. 14, p. 343.
[56] R. E. Peierls, Z. Phys. **80**, 763 (1933).
[57] C. W. J. Beenakker, arXiv:1907.06497.